

Local equilibrium in heavy-ion collisions. Microscopic analysis of a central cell versus infinite matter.

L. V. Bravina,^{1,2} E. E. Zabrodin,^{1,2} S. A. Bass,³ M. Bleicher,⁴ M. Brandstetter,⁵ S. Soff,⁵
H. Stöcker,⁵ and W. Greiner⁵

¹ *Institut für Theoretische Physik, Universität Tübingen, Auf der Morgenstelle 14, D-72076
Tübingen, Germany*

² *Institute for Nuclear Physics, Moscow State University, RU-119899 Moscow, Russia*

³ *National Superconducting Cyclotron Laboratory, Michigan State University, East Lansing,
Michigan 48823*

⁴ *Nuclear Science Division, Lawrence Berkeley Laboratory, Berkeley, California 94720*

⁵ *Institut für Theoretische Physik, Universität Frankfurt, Robert-Mayer-Str. 8-10, D-60325
Frankfurt, Germany*

Abstract

We study the local equilibrium in the central $V = 125 \text{ fm}^3$ cell in heavy-ion collisions at energies from $10.7A \text{ GeV}$ (AGS) to $160A \text{ GeV}$ (SPS) calculated in the microscopic transport model. In the present paper the hadron yields and energy spectra in the cell are compared with those of infinite nuclear matter, as calculated within the same model. The agreement between the spectra in the two systems is established for times $t \geq 10 \text{ fm}/c$ in the central cell. The cell results do not deviate noticeably from the infinite matter calculations with rising incident energy, in contrast to the apparent discrepancy with predictions of the statistical model (SM) of an ideal hadron gas. The entropy of this state is found to be very close to the maximum entropy, while hadron abundances and energy spectra differ significantly from those of the SM.

PACS numbers: 25.75.-q, 24.10.Lx, 24.10.Pa, 64.30.+t

I. INTRODUCTION

The hypothesis that local equilibrium (LE) can occur in the system of two heavy nuclei colliding head on at relativistic energies is one of the most intriguing problems in high-energy physics [1–18]. In this paper we continue to study the equilibration of hot and dense hadronic matter, produced in the central (with volume $V = 125 \text{ fm}^3$) cell in relativistic heavy-ion collisions, started in Ref. [19] (see also Refs. [20,21]). The equilibration of infinite nuclear matter has been studied separately in Refs. [22,23] and also in Ref. [24]. Here we will compare this idealized scenario to the properties of matter in the central cell of a heavy-ion collision. Both, the dynamics of the nuclear collisions in the energy range from from 10.7 to 160A GeV, as well as the infinite matter are calculated in the framework of the ultrarelativistic quantum molecular dynamics (UrQMD) model [25,26]. Note that in Ref. [24] hadron string dynamics (HSD) model [27] has been used for the infinite nuclear matter calculations.

The concept of local equilibrium assumes that for a given system a state is reached where all deviations of the system characteristics from the equilibrium ones can be treated as small perturbations. For instance, the distribution function of particles in the phase space $\{\vec{x}, \vec{p}\}$, $f(\vec{x}, \vec{p})$, can be approximated by

$$f(\vec{x}, \vec{p}) = f^{\text{eq}}(p) [1 + \Delta(\vec{x}, \vec{p})] \quad , \quad (1)$$

where $\Delta(\vec{x}, \vec{p}) \ll 1$ and $f^{\text{eq}}(p)$ is the equilibrium distribution function. But the central cell in a nuclear collision is an open system. Neither the energy density nor the particle composition in the cell is conserved. To decide whether or not the LE is attained in this open system the following procedure has been developed [19–21]. At the early stage of the collision the conditions of the *kinetic* equilibrium should be fulfilled. This implies the absence of significant (in the sense of LE definition) collective flow in the cell together with the nearly Maxwellian [see Eq. (1)] shape of particle momentum distributions. These conditions should be completed by the requirement of *thermal* and *chemical* equilibrium. It means that the particle energy spectra, $dN/4\pi p E dE$, and particle abundances should be close to those of equilibrated matter. In Refs. [19–21] the statistical model (SM) of an ideal hadron gas [22] with essentially the same hadron species as in the UrQMD model has been applied to calculate the characteristics of hadron-resonance matter in equilibrium. As an input the SM needs only three parameters, extracted from the microscopic calculations in the cell. Namely, the energy density ε , the baryon density ρ_B , and the strangeness density ρ_S , have to be determined. Solving then a system of nonlinear equations [19] one can reproduce particle yields and energy spectra in the SM via the temperature T , baryochemical potential μ_B , and strangeness chemical potential μ_S . If the spectra of hadrons in the microscopic cell calculations are close to the spectra predicted by the SM, the LE is assumed to set in in the cell.

The striking result of the investigations made in Ref. [19] is that the hot (and initially dense) hadron matter in the central cell does not reach the pure equilibrium in the sense of statistical mechanics during the time evolution, i.e., the state of maximum entropy [28]. However, it reaches the stage of kinetic equilibrium at time $t \cong 10 \text{ fm}/c$, almost irrespective of the energy of colliding nuclei. The deviations of the UrQMD results from the SM predictions become significant with rising center-of-mass energy of the system.

To make a final decision about the possibility of local equilibration in a heavy-ion collision, simulated within a microscopic model, the comparison with the equilibrated infinite matter, simulated within the same model, should be performed. This is essentially the subject of the present paper, which is organised as follows. A brief description of the model applied and the results on relaxation of the infinite hadron matter are given in Sec. II. After a certain nonstationary stage, yields and apparent temperatures of hadron species in the box with periodic boundary conditions, which models infinite matter, become time independent. This means that an equilibrium (or rather stationary) state is attained. Section III presents the comparison of the dynamical cell calculations with the stationary phase of infinite hadron matter. It is shown that the spectra in the cell at $t \geq 10$ fm/ c agree well with the infinite matter calculations, in contrast to the SM predictions. The discussion of the results obtained is given in Sec. IV. The origin of discrepancies between the UrQMD infinite matter simulations and the SM predictions is traced [21,22] to many-body ($N \geq 3$) decays of resonances and processes of multiparticle production via the excitation and fragmentation of quark-diquark (or quark-antiquark) strings. In the present paper we argue that the absorption of the excess of particle production (mainly pions) by the resonances, which can interact both inelastically and elastically within their lifetimes, is the key process which maintains the total balance of hadrons in the model calculations. The conclusions are drawn in Sec. V.

II. SIMULATION OF INFINITE HADRON MATTER

A. Initial conditions

To simulate the infinite hadron gas in the UrQMD model a cubic box of a volume $V = 5 \text{ fm} \times 5 \text{ fm} \times 5 \text{ fm} = 125 \text{ fm}^3$ with periodic boundary conditions has been chosen [22–25]. These conditions ensure that particles always remain in the box. For instance, if one particle crosses the face of the box and leaves it, another particle identical to the first one enters immediately the box from the opposite box face. The box plays a role of a heat bath in which the total energy density is conserved.

To define the initial state the number of particles, their composition and momenta must be specified. It can be a baryon-free gas of mesons, a baryon-antibaryon gas, or a gas of strings and resonances. For infinite nuclear matter with zero net strangeness and nonzero net baryon charge it is convenient to initialise a system consisting of protons and neutrons only [23]. Here the nucleons are uniformly distributed in the box volume. Their momenta are initialized randomly in a Fermi sphere with the subsequent rescaling to provide the required energy density. Further details concerning the simulations of infinite nuclear matter can be found elsewhere [22–24].

It is worth noting that such an analysis should not be mixed up with the study of dynamics of equilibration in relativistic heavy-ion collisions. In the latter case two Lorentz-contracted nuclei pass through each other and produce a nearly cylindrically expanding volume of hot and dense quark-hadron matter. The equilibration process in the central cell of such system proceeds faster compared to the box with the same values of energy density, baryon density and strangeness density. The cell is an open system and the most energetic particles leave it freely, causing an effective cooling of the rest of the hadron matter in the

cell. Times needed to reach thermal and chemical equilibration in the box (isolated system) are, apparently, much larger because of the permanent production of new particles in very energetic collisions at the nonequilibrium stage.

B. Equilibration in the box

Criteria of equilibrium of hot hadronic matter in the box [22,23] are similar to the criteria of equilibrium in the central cell of ultrarelativistic heavy-ion collisions, formulated in Refs. [19–21]. We recall them briefly. Conditions of *kinetic* equilibrium imply that (i) the velocity distributions $f_j(v)$ of hadron species j are isotropic and obey Maxwell distribution

$$f_j(v) \propto \exp\left(-\frac{m_j v^2}{2T}\right) \quad (2)$$

with T being the temperature of the system. For local equilibrium some deviations [see Eq. (1)] from the Maxwellian shape are possible. Therefore, it is convenient (especially for the central cell in heavy-ion collisions) to complete the verification procedure by (ii) the requirement of isotropy in the pressure sector. As a matter of fact, full isotropy of the velocity distributions leads obviously to the isotropy of the diagonal elements of the pressure tensor. Thus, criteria (i) and (ii) are not independent. But, instead of checking isotropy of the velocity distributions of all hadrons and their resonances in the box (or cell), it is more appropriate to confirm this isotropy for very few main hadron species, such as nucleons and pions, and then examine the isotropy of the integral distribution, such as pressure.

Since the number of particles is not a conserved quantity in strong interactions, the equilibrium in the system cannot be reached until abundances of all hadron species become saturated. Also, inelastic collisions affect the thermal distributions of particles. Therefore, criteria (i),(ii) should be completed by the requirement of time independence of (iii) energy distributions of particles (thermal equilibrium) and (iv) their yields (chemical equilibrium). Elastic scattering of particles drives the system to *thermal* equilibrium, while inelastic reactions push the system towards the stage of *chemical* equilibrium.

To examine the course of equilibration in the box the system of nucleons has been initialized. The values of the energy density, baryon density and strangeness density in the box are corresponding to those in the central cell with volume $V = 125 \text{ fm}^3$ in Pb+Pb central collision at SPS ($E_{\text{lab}} = 160A \text{ GeV}$) energy at time $t = 10 \text{ fm}/c$ after the beginning of the collision, namely, $\varepsilon = 468 \text{ GeV}/\text{fm}^3$, $\rho_B = 0.09 \text{ fm}^{-3}$, and $\rho_S = -0.01 \text{ fm}^{-3}$. At that time the hadronic matter in the cell is already in kinetic equilibrium [19,21]. As seen in Fig. 1 the second moments

$$\sigma_{x,y,z}^{(2)} = \langle v_{x,y,z}^2 \rangle - \langle v_{x,y,z} \rangle^2 \quad (3)$$

of the longitudinal and transverse velocity distributions of six main hadron species become isotropic after 50 fm/c. However, some of the hadron abundances are not frozen yet. Figure 2 depicts the evolution of the yields of π 's, K 's, \bar{K} 's, Δ 's, $(\Lambda + \Sigma)$'s, and N 's with time t . The saturation of the kaon yields is reached at about 70–90 fm/c after the beginning of the process, while the yields of other hadrons are saturated at 50–60 fm/c. These saturation

times agree with the results of Ref. [24], where the delay in saturation of the abundances of strange particles has been also observed.

The stationary stage, attained by the hadron matter in the box, is also characterised by a saturation of the number of inelastic and elastic collisions of hadrons and decays of resonances per unit of time. Figure 3 shows that about 45% of all reactions in the system are inelastic collisions. Another 27% of interactions are elastic, and the fraction of decays of resonances is about 28%. Compared with the number of resonance decays it means, particularly, that the rate of collisions is high and, therefore, more than 30% of all resonances suffer elastic or inelastic collisions with other hadrons within their lifetimes. According to Fig. 3 both elastic and inelastic reactions are controlled by meson-baryon (MB) and meson-meson (MM) interactions with small admixture of baryon-baryon (BB) collisions. Among the inelastic collisions the processes going via the formation of resonances (78% of the inelastic cross section) dominate over the reactions with the string formation (22% of σ_{inel}), as seen in Fig. 3(c).

At the initial nonequilibrium stage the collisions of hadrons are very energetic. Then, due to multiparticle processes, the kinetic energy of primordial nucleons is converted into the mass of newly produced particles, mainly mesons. As a result, the average energies of MM, MB and BB interactions, both elastic and inelastic, rapidly drop. The mean energy, $\langle\sqrt{s}\rangle$, of elastic and inelastic hadron collisions in the box at $t \geq 100$ fm/c is listed in Table I. The value of $\langle\sqrt{s}\rangle$ for elastic and inelastic collisions varies from 0.8 GeV for MM interactions up to 2.7 GeV for heavy BB systems. At these energies the contribution of elastic processes to the total cross section of a given reaction is indeed about 40% smaller than the inelastic cross section [29].

Figure 4 clarifies the kinetics of the equilibration of the pion yields, whose number can only be changed in inelastic reactions. The excess of pions produced in the fragmentation of strings is compensated by the absorption of pions by resonance matter, e.g., in a two-step process such as $\pi\pi \rightarrow \rho$ and $\rho\rho \rightarrow \pi\pi$. As mentioned before, because of the large particle density and large interaction cross section the resonances can interact immediately after their production without decay but, probably, with the formation of new strings. Thus the symmetry between the gain and loss terms for pions (as well as for other hadrons) is restored. Note, that although the chemical composition of the hadrons is frozen, the inelastic reactions in the system are not completely ceased.

To verify that not only chemical but also thermal equilibrium is attained the energy spectra of hadrons in the box have been studied. If the system is in thermal equilibrium these spectra should be nicely fitted to Gibbs distribution, $\exp(-E_i/T + \mu_i/T)$. Pion energy spectra, $dN/4\pi p E dE$, are shown at different times in Fig. 5(a), and nucleon energy spectra are represented in Fig. 5(b). Both spectra are remarkably close to the equilibrium fit. Nucleon energy spectra are time independent already after $t = 50$ fm/c with the ‘‘apparent’’ temperature $T_N \cong 127$ MeV, and the pion energy spectra become unchangeable at $t \approx 70$ fm/c, with the ‘‘apparent’’ temperature $T_\pi \cong 106$ MeV. The difference in T_π and T_N looks not very significant, $(T_N - T_\pi)/T_N \approx 0.17$. The hadronic matter in the box can be considered as a stationary system almost in equilibrium, since the conditions (i)–(iv) are satisfied.

III. COMPARISON BETWEEN CELL AND BOX RESULTS

A. Energy spectra and yields of hadrons

To compare the hadron yields and energy spectra in the central cell of heavy-ion collisions at energies 10.7 and 160A GeV with the hadronic spectra in equilibrium, the values of ε , ρ_B , and ρ_S have been extracted from the cell conditions at each time step. In Ref. [19] these values are substituted into the system of nonlinear equations of the statistical model to obtain temperature T , baryon chemical potential μ_B , and strangeness chemical potential μ_S . The procedure enables to calculate particle multiplicities and energy spectra in the SM.

In the present analysis the extracted parameters ε , ρ_B , ρ_S are used to initialize the system of hadrons in the box. The hadrons start to interact, elastically and inelastically, and the process of relaxation to the equilibrium begins. When the fluctuations of hadron yields and their energy spectra from some average values become small, and the average values themselves become time independent, the simulations are stopped. Then, the spectra of hadrons in the cell are compared with those of the infinite hadron matter. Energy spectra of hadron species in the cell at $t = 10$ fm/c are shown in Figs. 6(a) and 6(b) together with the box simulations for both energies. Predictions of the statistical model of an ideal hadron gas [22] are plotted as well. We see that the agreement between the cell and the box results is very good. It is insensitive to the rise of bombarding energy from AGS to SPS, in contrast to noticeable deviations from the predictions of SM. Values of the inverse slope parameter, extracted from the Boltzmann fit to particle spectra in the cell and in the box, and temperatures, given by the SM calculations, are listed in Table II for the central cell in Pb+Pb collisions at 160A GeV. The thermal characteristics of hadron species in the cell at $t \geq 10$ fm/c are close to those of the infinite nuclear matter, and rather far from the ideal equilibrium characteristics (see also Ref. [19]).

The abundances of hadrons in the cell for both reactions are presented in Figs. 7(a) and 7(b). The fractions of particles belonging to the final state of the heavy-ion collisions (“frozen” particles) are plotted onto the results also. Again, the yields of hadrons in the cell at $t \geq 10$ fm/c are close to the corresponding yields in the box for all species. Statistical model underestimates the number of pions, especially at high-energy densities, but provides a better agreement for the baryon sector. One can conclude that the hadron matter in the cell reaches at the late stage a quasiequilibrium state, similar to the state of infinite hadron matter simulated within the same microscopic model. This state is dubbed steady state [30,31]. On the other hand, the steady state does not match to the ideal thermal and chemical equilibrium, i.e., the state of maximum entropy. It means, particularly, that the conditions (i)–(iv) formulated in Sec. II are the necessary and sufficient criteria of the stationary (or steady) state only. Fulfilment of these conditions cannot guarantee thermal and chemical equilibration in the system of interacting hadrons from the point of view of equilibrium statistical mechanics.

The controversial point of the discussion is that the entropy of a statistical system should have a pronounced peak corresponding to the equilibrium configuration [28]. The experimentally measured mean multiplicities of secondaries in hadronic and nuclear collisions seem to agree roughly with the estimations of the SM, which links the multiplicity of the produced particles to the entropy of the thermalized system. Thus, the entropy of the steady state cannot be much smaller than the entropy given by the statistical model. To resolve the ambiguity it is important to study how much the entropy density in the cell deviates from

the maximum entropy density allowed to the system.

B. Entropy analysis

From here we will use s to denote the entropy density. For the statistical system of volume V in equilibrium the entropy density $s = S/V$ can be determined from the Gibbs thermodynamical identity

$$Ts = \varepsilon - \mu_B \rho_B - \mu_S \rho_S + P \quad , \quad (4)$$

where P denotes the pressure in the system. The alternative way is to define the entropy density via the particle distribution function $f(p, m_i)$:

$$s = - \sum_i \frac{g_i}{(2\pi\hbar)^3} \int_0^\infty f_i(p, m_i) [\ln f_i(p, m_i) - 1] d^3p \quad , \quad (5)$$

with g_i and m_i being the degeneracy factor and mass of the hadron species i , respectively. The last expression permits one to calculate the entropy density by means of the microscopic distribution function

$$f_i^{\text{mic}}(p) = \frac{(2\pi\hbar)^3 dN_i}{V g_i d^3p} \quad . \quad (6)$$

If the hadron cocktail reaches thermal and chemical equilibrium, the distribution functions of hadrons are given simply by Bose-Einstein or Fermi-Dirac distributions. In this case both Eqs. (4) and (5) should provide the same results for s . But: the hadron matter in the central cell (and in the box) is neither in chemical nor in thermal equilibrium at high energy densities. Therefore, the entropy densities calculated by Eq. (5) should be smaller than those predicted by the statistical model Eq. (4). This difference is clearly seen in Fig. 8, where the entropy densities per baryon, S/A , in the central cell at the quasiequilibrium stage are compared with the SM calculations. The S/A ratio in the cell is nearly constant during the late evolution of the system. Its deviation from the equilibrium value is about 4% at AGS and about 6–10% at SPS energy.

Partial entropy densities carried by nucleons and by pions in the central cell are shown in Fig. 9 together with the box and SM calculations. The entropies of hadron species in the cell appear to be very close to the equilibrium values, predicted by the SM, despite the difference in hadron abundances. For instance, although the number of pions in Pb+Pb collisions at SPS energy is twice as large in the cell at $t = 10$ fm/ c as in the ideal equilibrium [see Fig. 7(b)], the partial entropy densities are nearly the same, $s_\pi^{\text{mic}} \cong s_\pi^{\text{SM}}$. This is due to the fact that the apparent temperature of pions in the cell is much lower than the SM temperature listed in Table II. Therefore, the total entropy of the steady state, attained by the hadron matter in the central cell or by the infinite hadron matter, is close to the maximum entropy, assigned to the system in thermal and chemical equilibrium.

IV. WHICH EQUILIBRIUM IS TRUE?

In Ref. [19] it was shown that the hadronic yields and energy spectra in the central cell of relativistic heavy-ion collisions do not coincide with the corresponding spectra, given by

the SM, not even at the stage of kinetic equilibrium. Formally this means that thermal and chemical equilibrium in the cell is not reached yet. For instance, times $t \leq 20$ fm/ c may be too short compared to the typical equilibration times.

The present study reveals, however, that the hadron distributions in the cell after $t \cong 10$ fm/ c agree well with the hadron spectra of infinite hadron matter, simulated within the same microscopic model. At relatively low energy densities the results of the box simulations are close to the predictions of the statistical model. The accord is broken at energy densities higher than 0.5 GeV/fm³. Which equilibrium is true and what is the origin of the disagreement? To answer these questions it is necessary to analyse the temperatures of the hadron species in the box as a function of energy density. Figure 10 presents the UrQMD simulations in the cell and in the box together with the SM estimates for Pb+Pb collisions at $160A$ GeV. At the high density phase of a heavy-ion collision the cell results exhibit dramatic deviations both from the SM and from the box calculations. After $t \geq 10$ fm/ c (cell time only) the difference between the box and the cell data is small. But both microscopic model simulations diverge clearly from the predictions of the statistical model. As was noticed in Ref. [22], the $T(\varepsilon)$ dependence in the UrQMD box is the same as in the SM if the multiparticle processes $2 \rightarrow N$ ($N \geq 3$) and the many-body decays of resonances have ceased in the system. This explains the agreement between the two models at low-energy densities. At high energy densities the microscopic model predicts the appearance of limiting temperatures similar to that of the statistical bootstrap model [3] for each of the hadron species. These temperatures lie within the range $105 \text{ MeV} \leq T_{\text{lim}} \leq 145 \text{ MeV}$ [19,22,23]. Slightly higher limiting temperature $T_{\text{lim}} = 150 \pm 5 \text{ MeV}$ has been found in Ref. [24]. The deviations in model calculations can be attributed to a different number of hadron species, which is higher in the UrQMD, and to different threshold of the excitation of strings [24]. Although the temperatures of hadrons are relatively close to each other, the whole system is not characterised by a unique temperature. Therefore, the system is not in the conventional thermal equilibrium.

The chemical composition of the hadron system in the box freezes after a while (see Sec. II). The excess of hadrons, mainly pions, produced in inelastic collisions is absorbed by the resonance matter. For instance, the reaction $N\pi \rightarrow N\pi\pi$ may be compensated by a two-step process $N\pi \rightarrow \Delta$ and $\pi\Delta \rightarrow N\pi$ (this is only a simplified example, the real number of production and absorption channels is > 100). Does it mean that the conditions of equilibrium are fulfilled? The striking answer is **no**, because the chemical equilibrium assumes unambiguously that the rates of every coupled direct and inverse reaction in equilibrium must be the same [28,32]. The cyclic process during which the system transforms from the quantum state \mathcal{L} to quantum state \mathcal{K} and then comes back to the initial state \mathcal{L} via an intermediate state \mathcal{M} violates the necessary conditions of equilibrium [32]. Thus, although the yields of hadrons are time independent, the system is not in chemical equilibrium, as defined by equilibrium statistical mechanics.

It is important to explain the difference between the evolution scenarios predicted by the hydrodynamic and microscopic models for the heavy-ion collisions at ultrarelativistic energies. According to typical hydrodynamic picture [33], the system of hadrons is produced in chemical and thermal equilibrium shortly after the QGP hadronization. Because of the expansion of the system its temperature, energy density and particle density drop. The mean free path for inelastic collisions grows much faster than that for the elastic ones. For

instance, the mean free path for inelastic and elastic $\pi\pi$ collisions increases with the power T^{-9} and T^{-5} , respectively [34]. Chemical freeze-out takes place when the mean free path for inelastic collisions becomes comparable with the radius of the fireball, i.e., significantly earlier than the thermal freeze-out. After the (sequential) chemical freeze-out the system quickly gets out of chemical equilibrium, heavy resonances decay and chemical potentials start to develop [33]. The thermal equilibrium is maintained until the thermal freeze-out, when the mean free path of elastic collisions rises above the linear dimensions of the system.

The altered scenario is provided by the microscopic model simulations. Here the system of hadrons in the central cell at $t \geq 10$ fm/ c is neither in chemical nor in thermal equilibrium. Despite the fact that hadron abundances are frozen, competing inelastic processes take place still. Also, the temperatures of hadron species are different but quite stable, as shown by the simulations of the infinite nuclear matter.

Although it is still questionable whether or not the microscopic hadron-string models can adequately describe the early stage of ultrarelativistic heavy-ion collisions, these models are really good in description of the late hadronic phase until the freeze-out of particles. It is the late stage of heavy-ion collisions that is studied in the microscopic transport model in the present paper. The rates of elastic and inelastic processes in the box with the values of ε , ρ_B and ρ_S corresponding to those of the central cell in heavy-ion collisions at AGS and SPS energies at the stage of kinetic equilibrium are listed in Table III. The number of processes going via the string formation is rather small (less than 10%) compared to the number of elastic reactions and to the number of processes with the formation and decay of resonances. It is easy to see that the total balance of particles is fulfilled, i.e., 2.47 (34.35) particles per fm/ c are produced in the decays of resonances and strings, and essentially the same 2.47 (34.28) particles per fm/ c are absorbed by resonance matter in the box with AGS (SPS) cell conditions. The mean total energy per hadron, 1.0 ± 0.1 GeV (see Table I), is equal to the value 1 GeV of the mean total energy per hadron at chemical freeze-out, estimated from the statistical model fit to various experimental data from several GeV up to few hundred GeV per nucleon (see, e.g., [17] and references herein). But the hadron content and the temperatures are far from those given by the SM. This difference arise because of the lack of inverse reactions, $N \rightarrow 2$, which are not included in any of the available microscopic models designed for the description of heavy-ion collisions.

V. CONCLUSIONS

The results may be summarized as follows. The microscopic transport UrQMD model is employed to study the appearance of local equilibrium in the central cell of heavy-ion collisions at relativistic energies from 10.7 to 160A GeV. The hadron spectra in the cell are compared with the corresponding spectra of the infinite nuclear matter, reproduced in a box with periodic boundary conditions [22,23] within the same microscopic model. A comparison with the predictions of the statistical model of an ideal hadron gas has been done in Ref. [19] in detail.

The yields and energy spectra of hadrons in the cell at $t \geq 10$ fm/ c are found to be close to those in the box irrespective of the c.m. energy of colliding nuclei. The late hadron matter in the UrQMD cell, therefore, reaches a quasiequilibrium stage, dubbed steady state

[30,31]. On the other hand, the steady state of hadron matter even at not very high-energy densities differs from the idealised equilibrium state assumed by the SM.

The total entropy density is close to the maximum entropy density given by the SM. At SPS energy, for instance, the difference is not too large, $(s_{\text{tot}}^{\text{SM}} - s_{\text{tot}}^{\text{mic}})/s_{\text{tot}}^{\text{SM}} \cong 6\%$ only. Moreover, the entropy per baryon in the cell remains constant in the time interval $10 \leq t \leq 20$ fm/ c for energies varying from 10.7 to 160A GeV. This explains why the rapidity distribution of secondaries in hadronic and nuclear interactions, predicted by hydrodynamic models at those energies, fits well to the experimental data.

However, the hadrons in the UrQMD steady state do not exhibit a universal temperature for all species. The yields of mesons, especially pions, deviate from the calculations with the SM. It has been verified previously [19] that the assumption of a “partial” thermalization of all hadron species except pions cannot improve the quality of the fit to the SM. Elimination of pions causes the rise of the strangeness chemical potential [19], but not the decrease of the temperature of baryons.

The origin of the deviations is traced to different rates of direct and inverse reactions for the multiparticle processes and many-body decays of resonances, as well as nonzero lifetimes of the resonances. Absence of the reactions $N \rightarrow 2$ and $N \rightarrow 1$ ($N \geq 3$), which is a feature of all microscopic models, leads to appearance of a cyclic process in the microscopic calculations. The cyclic process where, e.g., pions are produced in inelastic collisions and then are absorbed by resonance matter, violates the equivalence of rates of every coupled direct and inverse reaction, which is the basic principle of the equilibrium statistical mechanics.

ACKNOWLEDGMENTS

We would like to thank L. Csernai, M. Gyulassy, Amand Faessler, and E. Shuryak for the stimulating discussions and valuable comments. This work was supported by the Graduiertenkolleg für Theoretische und Experimentelle Schwerionenphysik, Frankfurt–Giessen, the Bundesministerium für Bildung und Forschung, the Gesellschaft für Schwerionenforschung, Darmstadt, Deutsche Forschungsgemeinschaft, and the Alexander von Humboldt-Stiftung, Bonn. S.A.B. acknowledges financial support from the U.S. National Science Foundation, Grant No. PHY-9605207.

REFERENCES

- [1] E. Fermi, Prog. Theor. Phys. **5**, 570 (1950); Phys. Rev. **81**, 683 (1951).
- [2] L.D. Landau, Izv. Akad. Nauk SSSR, Ser. Fiz. **17**, 51 (1953) [*Collected papers of L.D. Landau*, edited by D. Ter Haar (Gordon and Breach, New York, 1965), p.569]; S.Z. Belenkij and L.D. Landau, Nuovo Cimento Suppl. **3**, 15 (1956).
- [3] R. Hagedorn, Suppl. Nuovo Cimento **3**, 147 (1965);
R. Hagedorn and J. Rafelski, Phys. Lett. **97B**, 136 (1980).
- [4] E.V. Shuryak, Phys. Rep. **61**, 71 (1980); Nucl. Phys. **A661**, 119c (1999).
- [5] J.D. Bjorken, Phys. Rev. D **27**, 140 (1983).
- [6] *Local Equilibrium in Strong Interaction Physics*, edited by D.K. Scott and R.M. Weiner (World Scientific, Singapore, 1985).
- [7] H. Stöcker and W. Greiner, Phys. Rep. **137**, 277 (1986).
- [8] K. Geiger and J.I. Kapusta, Phys. Rev. D **47**, 4905 (1993).
- [9] K. Geiger, Phys. Rep. **258**, 237 (1995).
- [10] W. Cassing, V. Metag, U. Mosel, and K. Niita, Phys. Rep. **188**, 363 (1990).
- [11] P. Braun-Munzinger, J. Stachel, J.P. Wessels, and N. Xu, Phys. Lett. B **365**, 1 (1996).
- [12] S.A. Bass, M. Belkacem, M. Brandstetter, M. Bleicher, L. Gerland, J. Konopka, L. Neise, C. Spieles, S. Soff, H. Weber, H. Stöcker, and W. Greiner, Phys. Rev. Lett. **81**, 4092 (1998).
- [13] M. Bleicher, M. Belkacem, C. Ernst, H. Weber, L. Gerland, C. Spieles, S.A. Bass, H. Stöcker, and W. Greiner, Phys. Lett. B **435**, 9 (1998).
- [14] F. Becattini, M. Gazdzicki, and J. Sollfrank, Eur. Phys. J. C **5**, 143 (1998).
- [15] U. Heinz, J. Phys. G **25**, 263 (1999); Nucl. Phys. **A661**, 140c (1999).
- [16] J. Letessier and J. Rafelski, J. Phys. G **25**, 451 (1999); Phys. Rev. C **59**, 947 (1999).
- [17] J. Cleymans and K. Redlich, Phys. Rev. C **60**, 054908 (1999); J. Cleymans, H. Oeschler, and K. Redlich, J. Phys. G **25**, 281 (1999).
- [18] J. Sollfrank, U. Heinz, H. Sorge, and N. Xu, Phys. Rev. C **59**, 1637 (1999).
- [19] L.V. Bravina, E.E. Zabrodin, M.I. Gorenstein, S.A. Bass, M. Belkacem, M. Bleicher, M. Brandstetter, C. Ernst, M. Hoffman, L. Neise, S. Soff, H. Weber, H. Stöcker, and W. Greiner, Phys. Rev. C **60**, 024904 (1999).
- [20] L.V. Bravina, M.I. Gorenstein, M. Belkacem, S.A. Bass, M. Bleicher, M. Brandstetter, M. Hoffman, S. Soff, C. Spieles, H. Weber, H. Stöcker, and W. Greiner, Phys. Lett. B **434**, 379 (1998).
- [21] L.V. Bravina, M. Brandstetter, M.I. Gorenstein, E.E. Zabrodin, M. Belkacem, M. Bleicher, S.A. Bass, C. Ernst, M. Hofmann, S. Soff, H. Stöcker, and W. Greiner, J. Phys. G **25**, 351 (1999).
- [22] M. Belkacem, M. Brandstetter, S.A. Bass, M. Bleicher, L. Bravina, M.I. Gorenstein, J. Konopka, L. Neise, C. Spieles, S. Soff, H. Weber, H. Stöcker, and W. Greiner, Phys. Rev. C **58**, 1727 (1998).
- [23] M. Brandstetter *et al.* (unpublished).
- [24] E.L. Bratkovskaya, W. Cassing, C. Greiner, M. Effenberger, U. Mosel, and A. Sibirtsev, Nucl. Phys. **A675**, 661 (2000).
- [25] S.A. Bass, M. Belkacem, M. Bleicher, M. Brandstetter, L. Bravina, C. Ernst, L. Gerland, M. Hofmann, S. Hofmann, J. Konopka, G. Mao, L. Neise, S. Soff, C. Spieles, H. Weber,

- L.A. Winckelmann, H. Stöcker, W. Greiner, Ch. Hartnack, J. Aichelin, and N. Amelin, Prog. Part. Nucl. Phys. **41**, 255 (1998).
- [26] M. Bleicher, E. Zabrodin, C. Spieles, S.A. Bass, C. Ernst, S. Soff, L. Bravina, M. Belkacem, H. Weber, H. Stöcker, and W. Greiner, J. Phys. G **25**, 1859 (1999).
- [27] W. Eehalt and W. Cassing, Nucl. Phys. **A602**, 449 (1996).
- [28] L.D. Landau, E.M. Lifshitz, and L.P. Pitaevskii, *Statistical Physics* (Pergamon, New York, 1980), Pt. 1.
- [29] R.M. Barnett *et al.*, Particle Data Group, Phys. Rev. D **54**, 1 (1996).
- [30] D. Kondepudi and I. Prigogine, *Modern Thermodynamics: From Heat Engines to Dissipative Structures* (Wiley, Chichester, 1998).
- [31] E.E. Zabrodin, L.V. Bravina, H. Stöcker, and W. Greiner, hep-ph/9901356.
- [32] R.C. Tolman, *The Principles of Statistical Mechanics* (Oxford University Press, Oxford, 1967), p. 522.
- [33] H. Bebie, P. Gerber, J.L. Goity, and H. Leutwyler, Nucl. Phys. **B378**, 95 (1992).
- [34] P. Gerber, J.L. Goity, and H. Leutwyler, Phys. Lett. B **246**, 513 (1990).

FIGURES

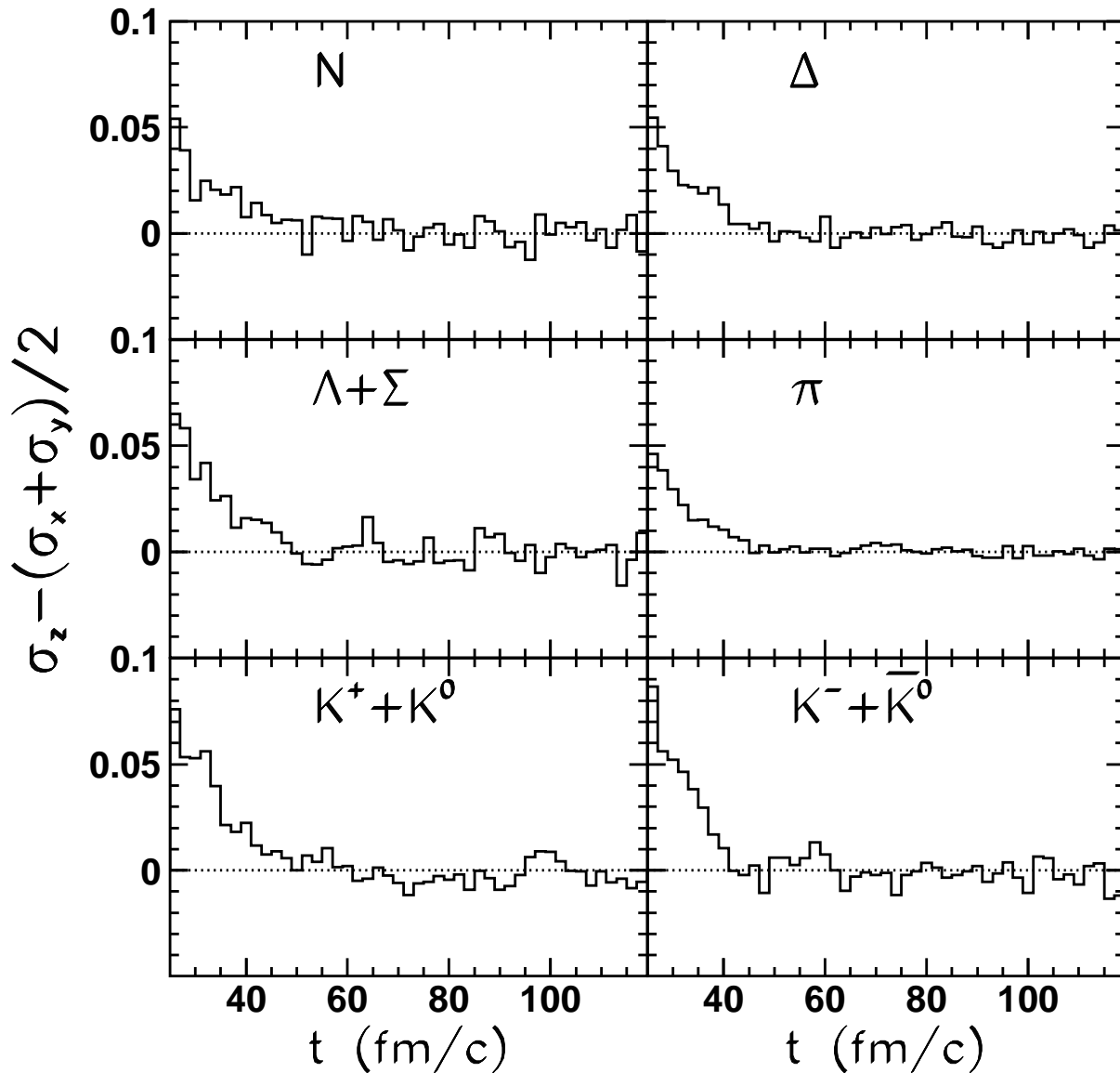


FIG. 1. Anisotropy function $f_a^{(2)} = \sigma_z^{(2)} - (\sigma_x^{(2)} + \sigma_y^{(2)})/2$ of the velocity distributions of hadron species in the box with volume $V = 125 \text{ fm}^3$ as a function of time. Conditions in the box correspond to those of the central $V = 125 \text{ fm}^3$ cell in central Pb+Pb collision at 160A GeV at $t = 10 \text{ fm}/c$, i.e., $\varepsilon = 468 \text{ MeV}/\text{fm}^3$, $\rho_B = 0.0924 \text{ fm}^{-3}$, and $\rho_S = -0.00987 \text{ fm}^{-3}$.

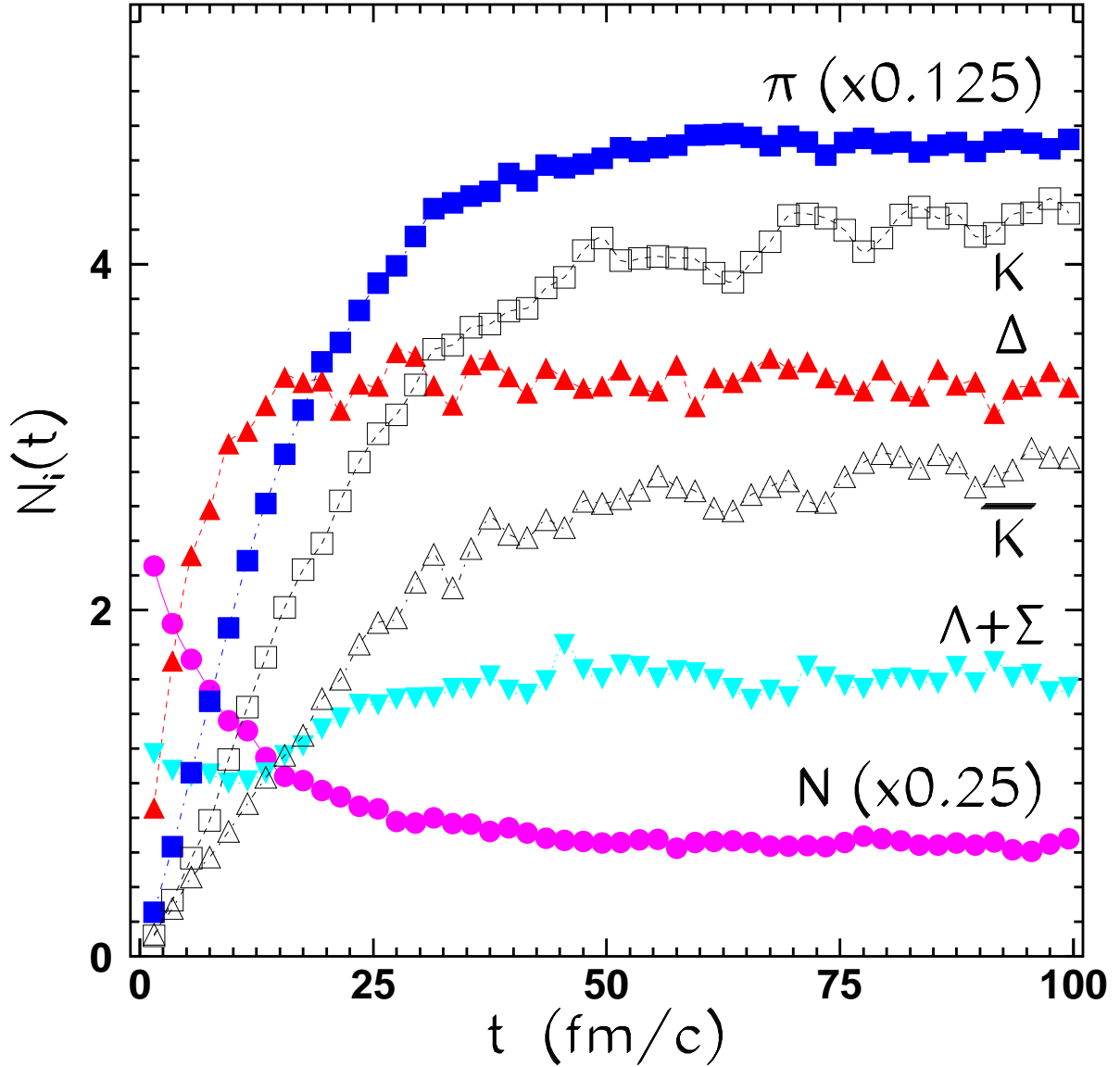


FIG. 2. Time evolution of the yields of π 's, K 's, \bar{K} 's, N 's, $(\Lambda + \Sigma)$'s and Δ 's in the box with $V = 125 \text{ fm}^3$, $\varepsilon = 468 \text{ MeV/fm}^3$, $\rho_B = 0.0924 \text{ fm}^{-3}$, and $\rho_S = -0.00987 \text{ fm}^{-3}$.

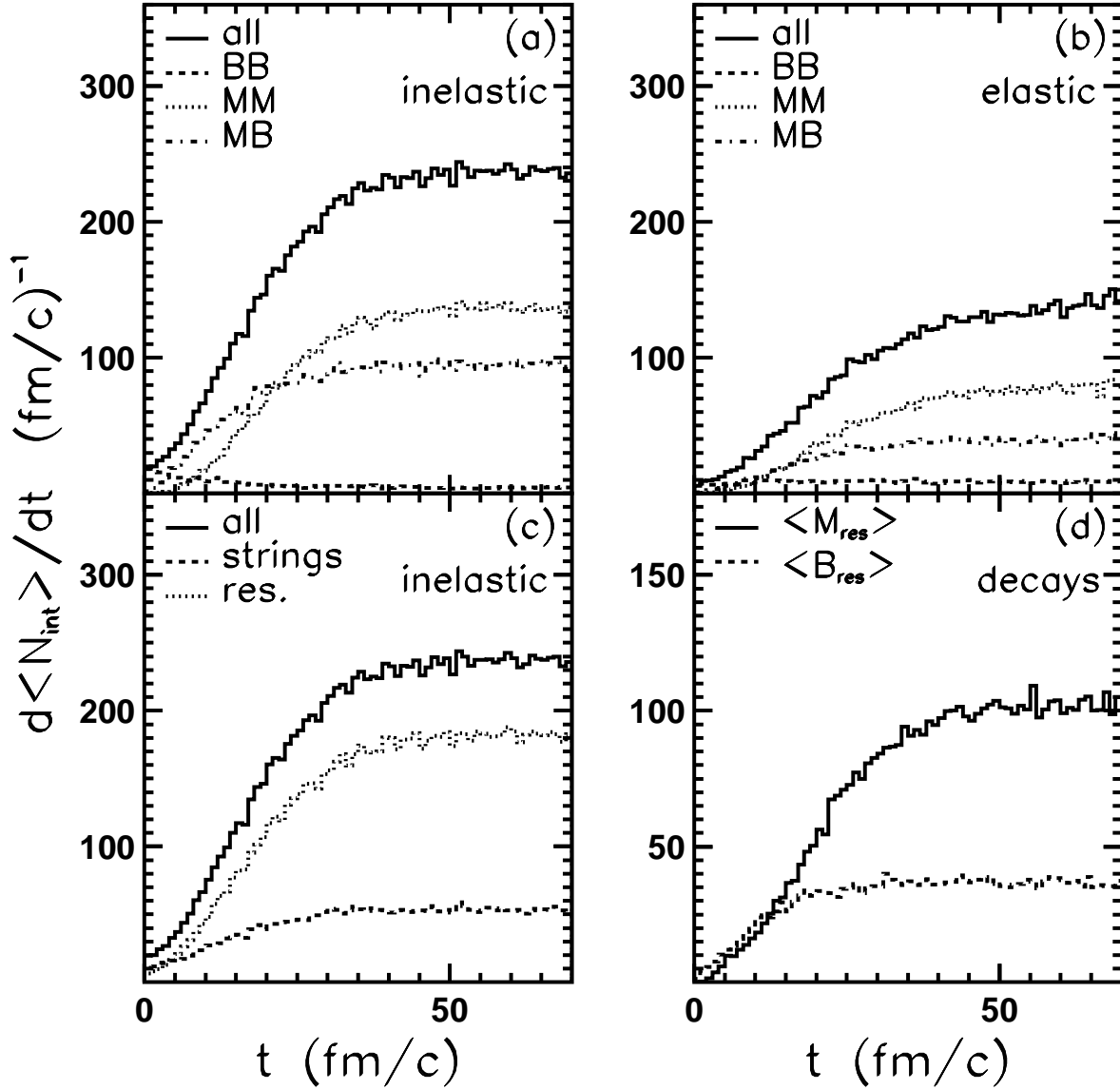


FIG. 3. Time evolution of the number of inelastic (a),(c) and elastic (b) collisions, and decays of resonances (d) in the box with $V = 125 \text{ fm}^3$, $\varepsilon = 468 \text{ MeV}/\text{fm}^3$, $\rho_B = 0.0924 \text{ fm}^{-3}$, and $\rho_S = -0.00987 \text{ fm}^{-3}$.

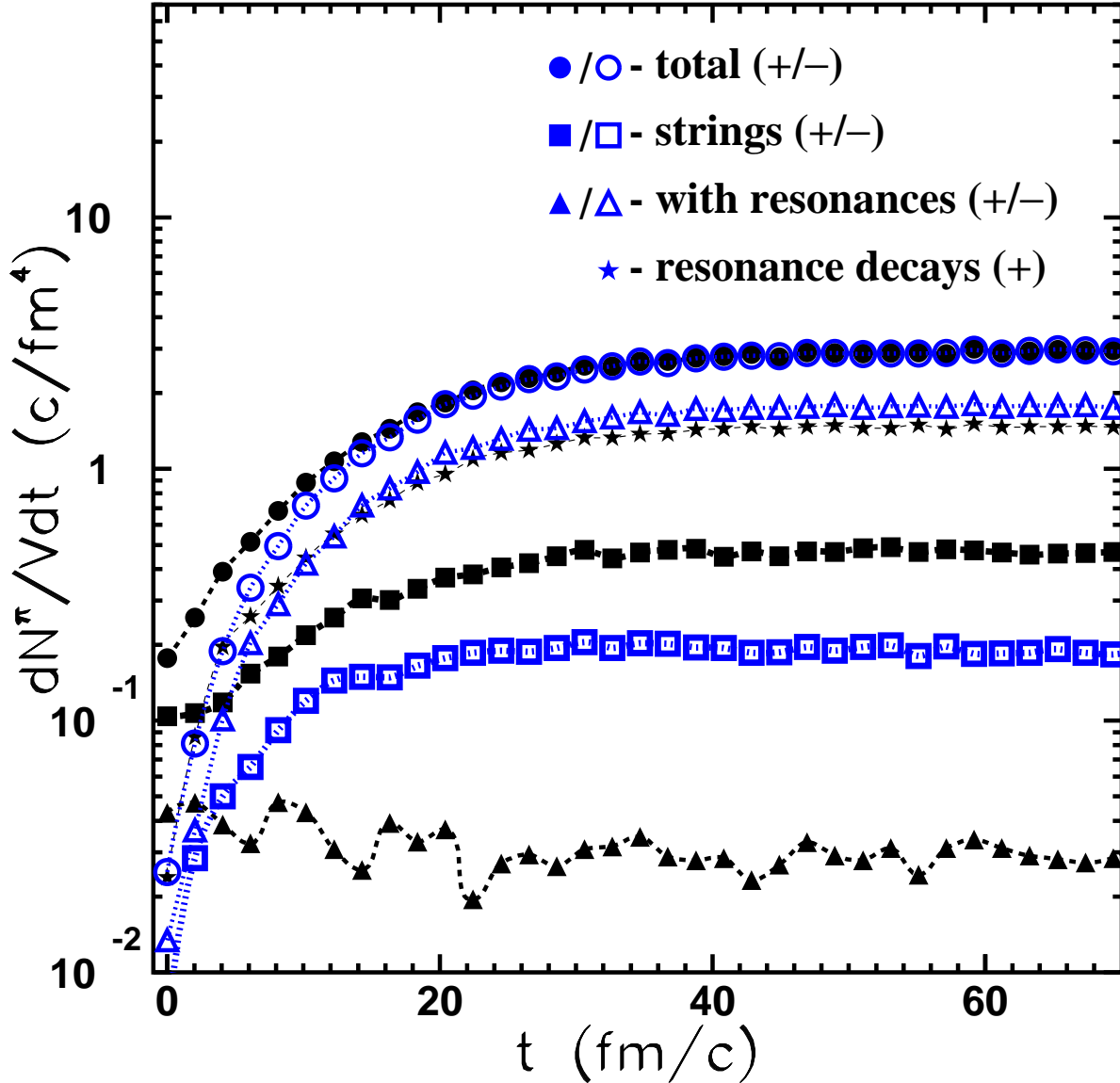


FIG. 4. Production rates for pions in the box with $V = 125 \text{ fm}^3$, $\varepsilon = 468 \text{ MeV/fm}^3$, $\rho_B = 0.0924 \text{ fm}^{-3}$, and $\rho_S = -0.00987 \text{ fm}^{-3}$. Pions are produced (full symbols) and absorbed (open symbols) in various inelastic processes, including break-up and formation of strings (boxes), and reactions with resonance excitations (triangles). Pions coming directly from the decays of resonances are shown by stars.

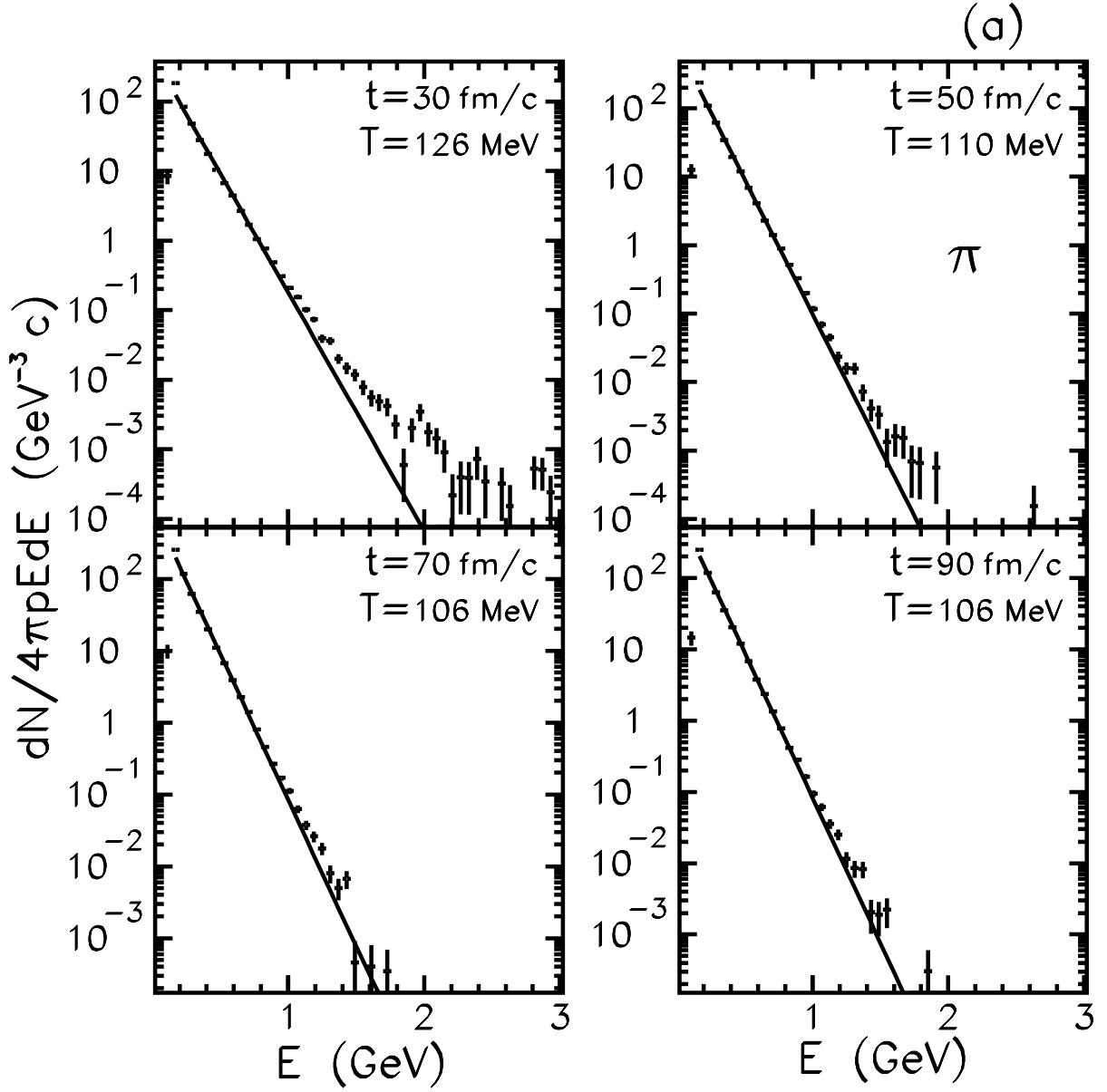
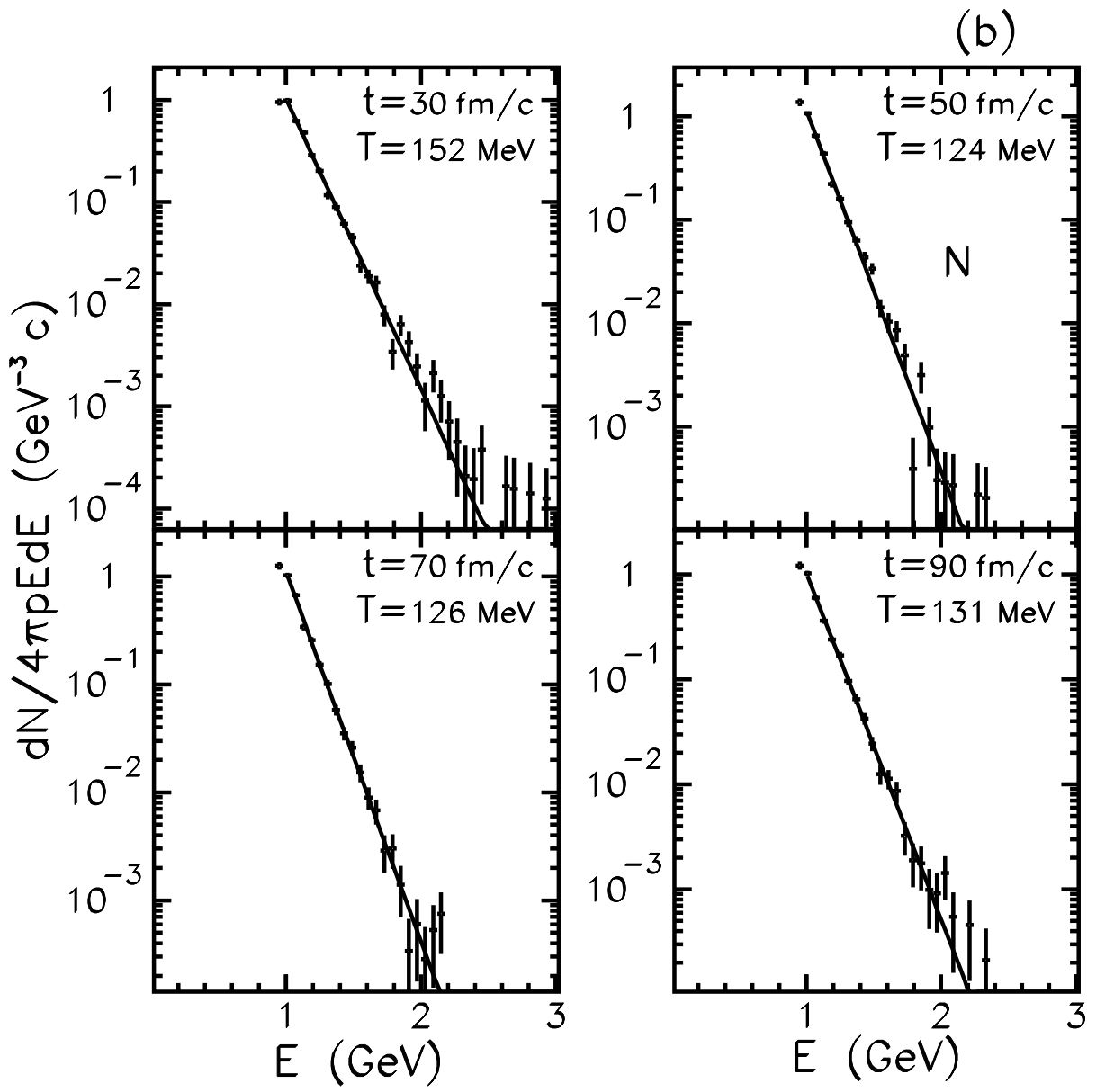


FIG. 5. (a) Time evolution of the energy spectra of pions in the box with $V = 125 \text{ fm}^3$, $\varepsilon = 468 \text{ MeV}/\text{fm}^3$, $\rho_B = 0.0924 \text{ fm}^{-3}$, and $\rho_S = -0.00987 \text{ fm}^{-3}$. Solid lines are the results of Boltzmann fit to the distributions. The value of the inverse slope parameter, T , is listed in each panel of the figure. (b) The same as (a) but for nucleon energy spectra in the box.



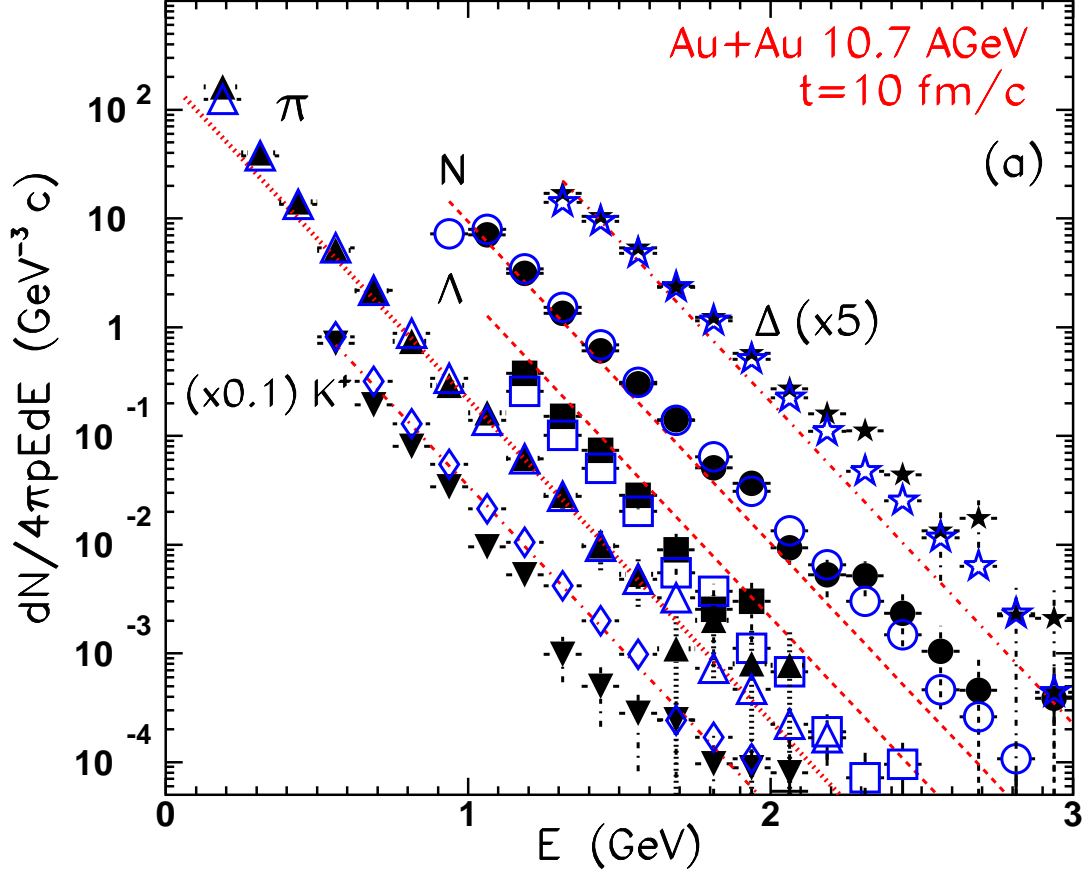
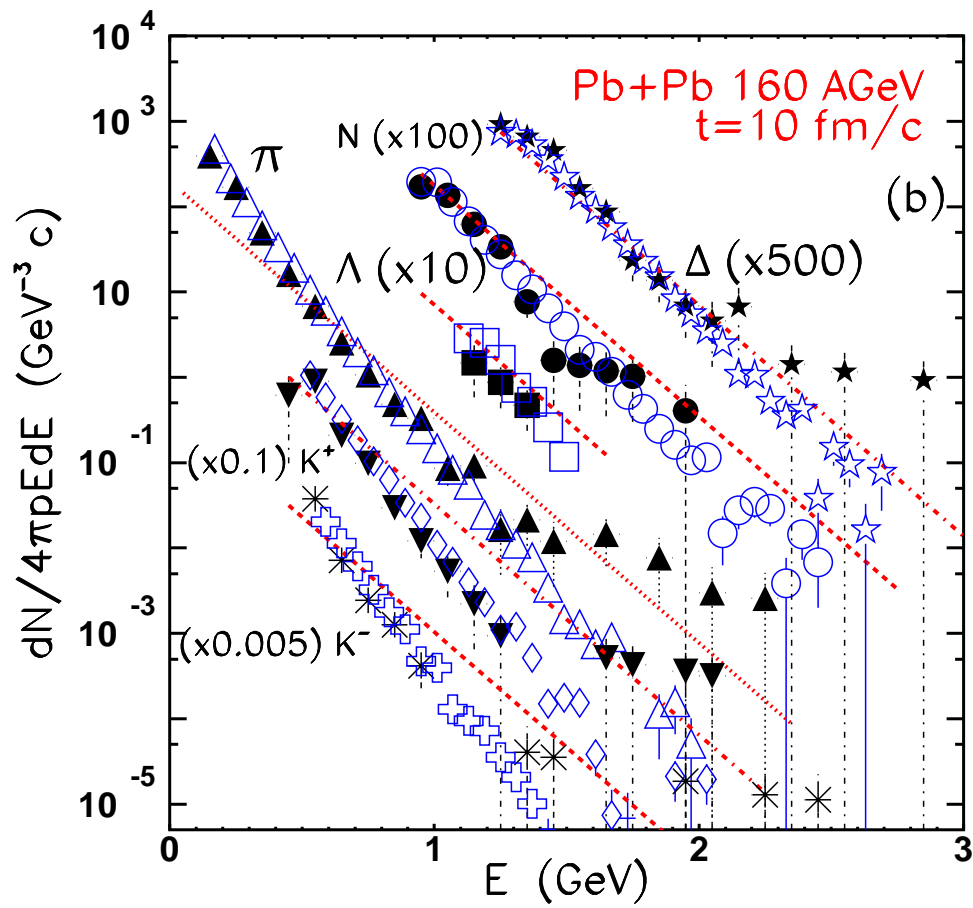


FIG. 6. (a) Energy spectra of N (circles), Λ (boxes), π (triangles up), K^+ (triangles down and diamonds), and Δ (stars) in the central 125 fm^3 cell of Au+Au collisions at $10.7A \text{ GeV}$ at $t=10 \text{ fm}/c$. Open symbols indicate UrQMD box calculations. Lines are the results of Boltzmann fit to the distributions with the parameters $T=147 \text{ MeV}$, $\mu_B=510 \text{ MeV}$, $\mu_S=129 \text{ MeV}$ obtained in the ideal hadron gas model. (b) The same as (a) but for Pb+Pb collisions at $160A \text{ GeV}$. In addition, spectra of K^- 's (asterisks and open crosses) are plotted. Parameters of the Boltzmann fit are $T=161 \text{ MeV}$, $\mu_B=197 \text{ MeV}$, $\mu_S=36.8 \text{ MeV}$.



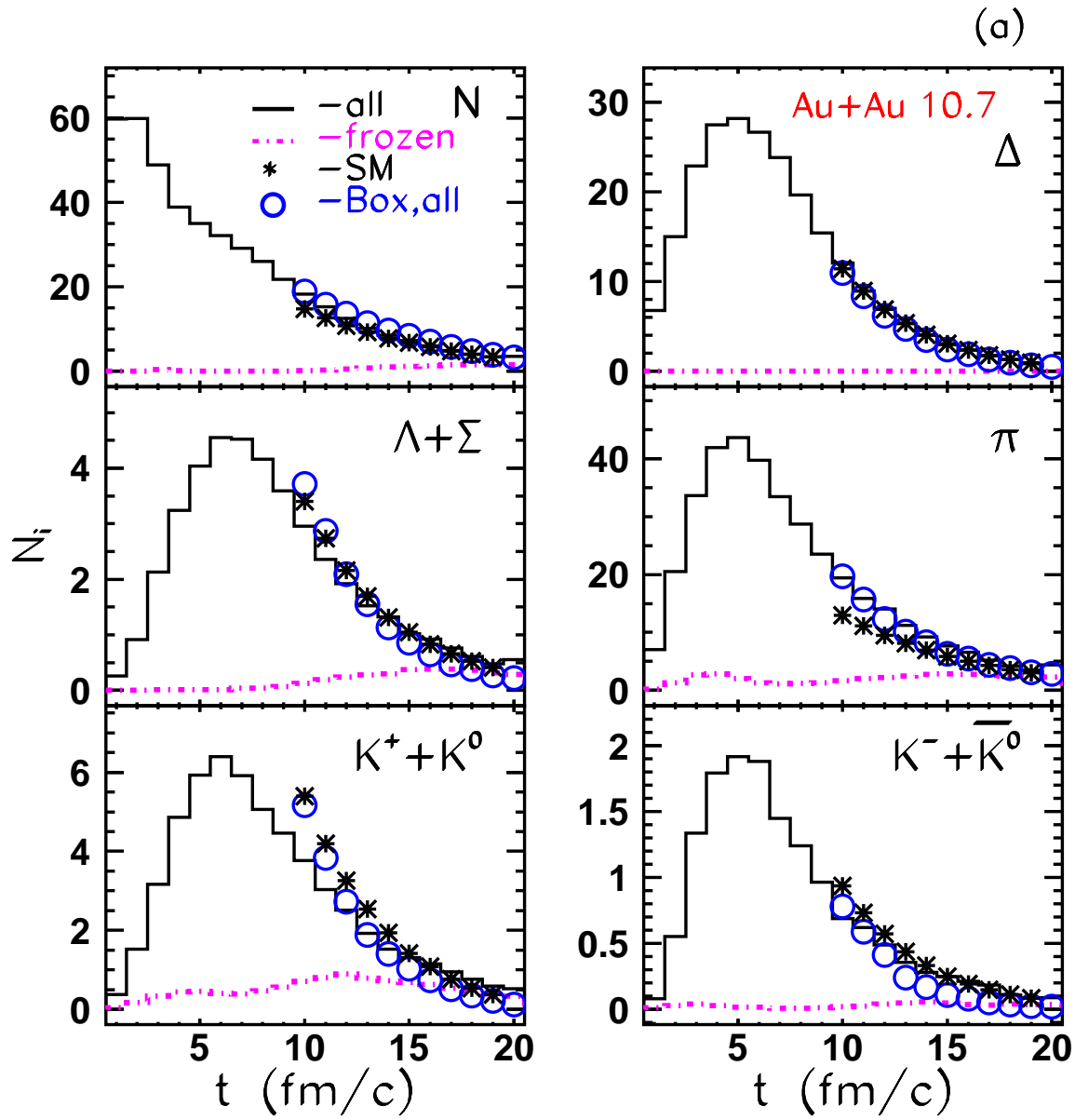
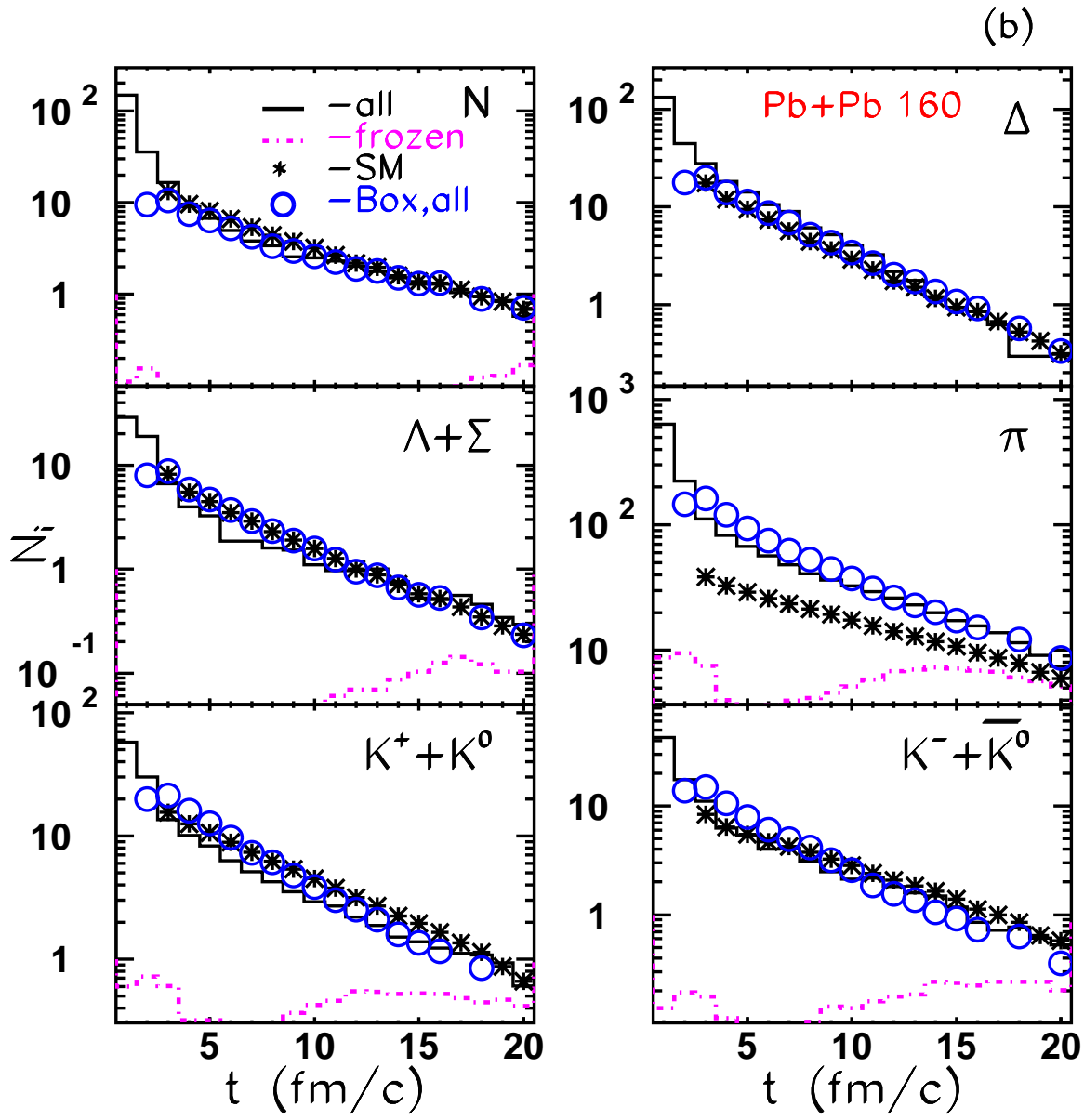


FIG. 7. (a) The number of particles in the central cell of heavy-ion collisions at $10.7A$ GeV as a function of time as obtained in the UrQMD model (histograms) together with the predictions of the SM (asterisks) and with the box calculations (open circles). The fractions of frozen particles in the cell are shown by dot-dashed lines. (b) The same as (a) but for Pb+Pb collisions at $160A$ GeV.



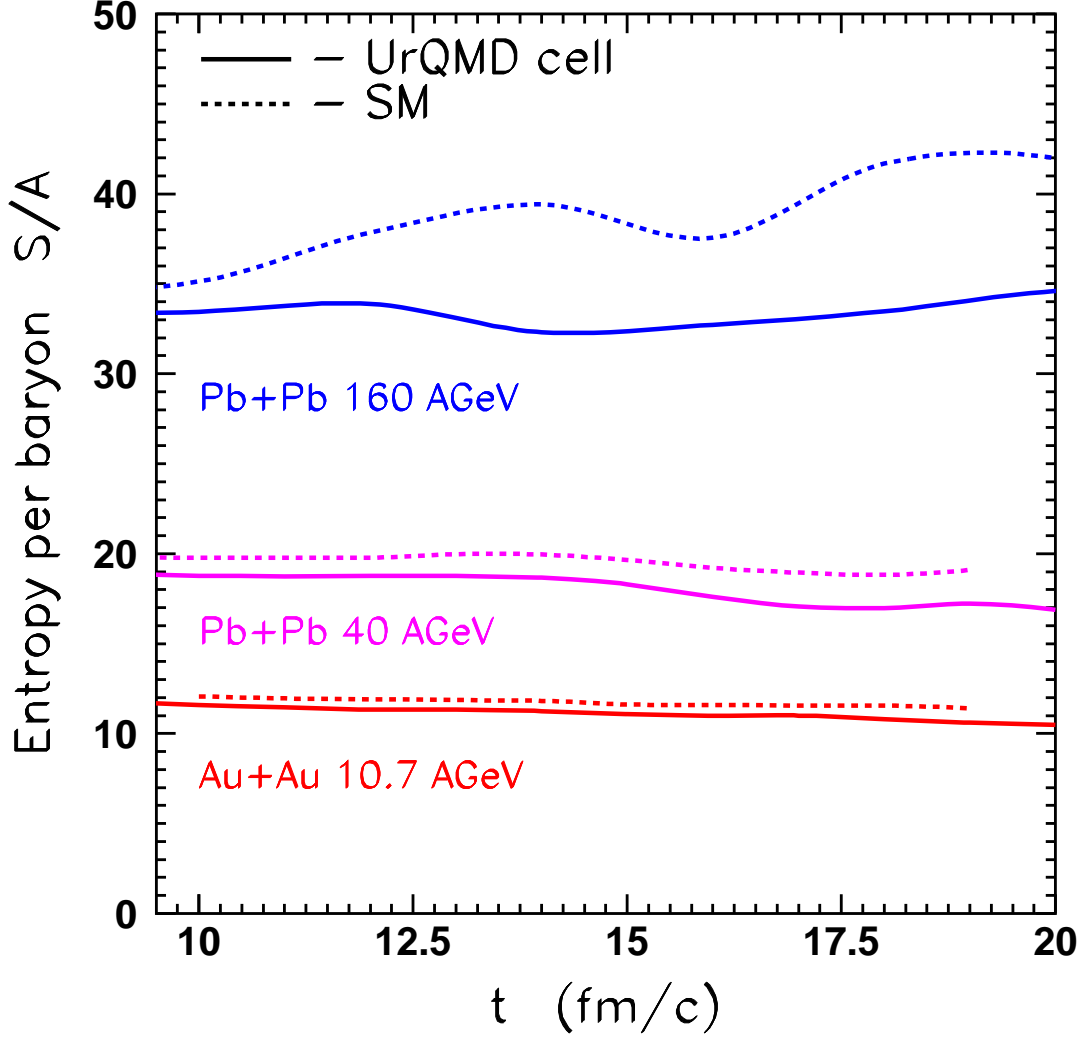


FIG. 8. Time evolution of the entropy per baryon ratio, S/A , in the central cell with $V = 125 \text{ fm}^3$ in heavy-ion collisions at 10.7, 40, and 160A GeV. Solid lines indicate microscopic calculations with the UrQMD model. Dashed lines show the predictions of the SM of an ideal hadron gas, obtained with the same values of baryon density, energy density and strange density, as extracted from the analysis of the cell conditions in the UrQMD simulations.

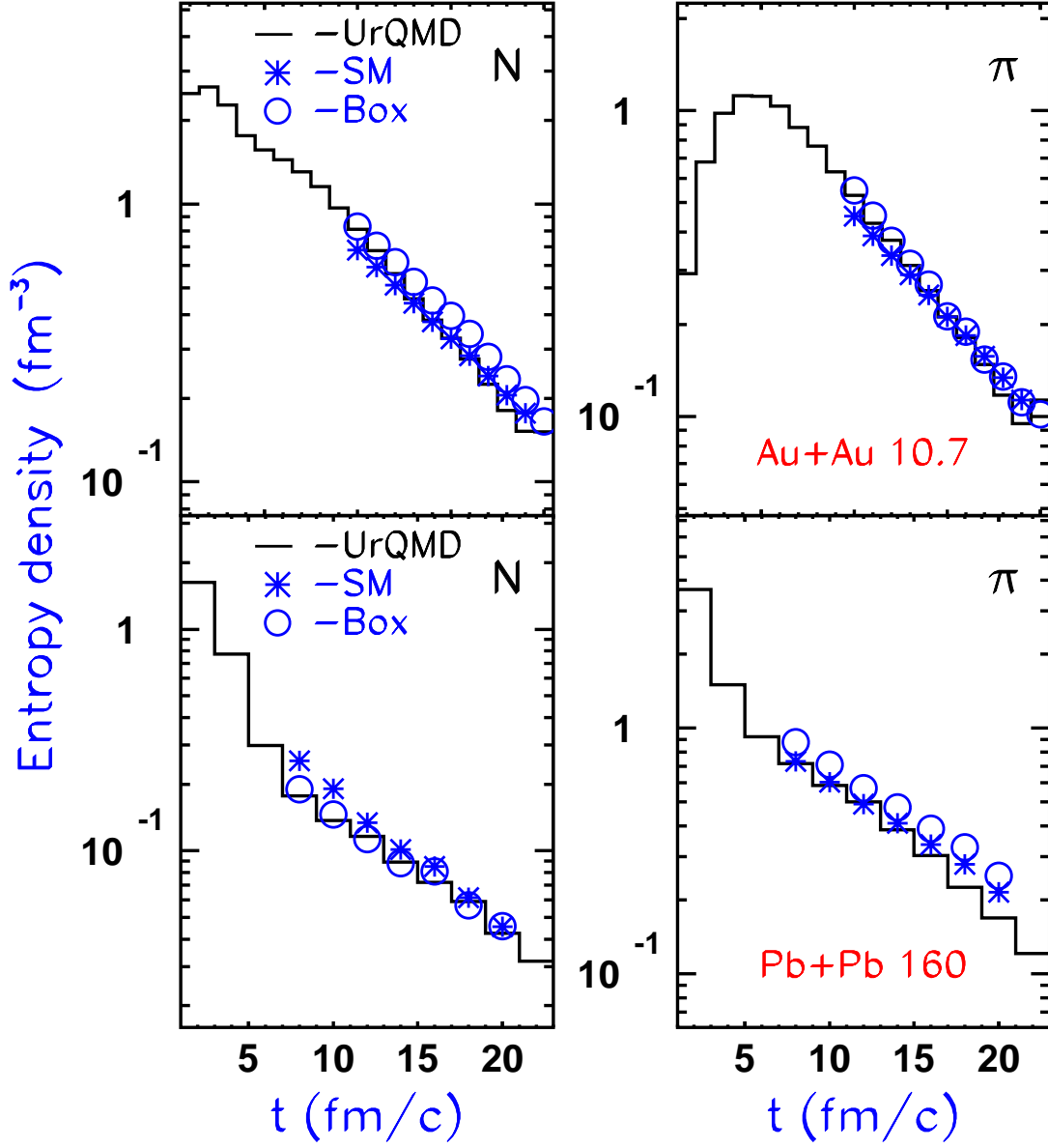


FIG. 9. Partial entropy densities of N 's and π 's in the central cell of heavy-ion collisions at 10.7A GeV (upper panels) and 160A GeV (lower panels). Histograms denote the UrQMD simulations. Predictions of the SM and box calculations are shown by asterisks and by open circles, respectively.

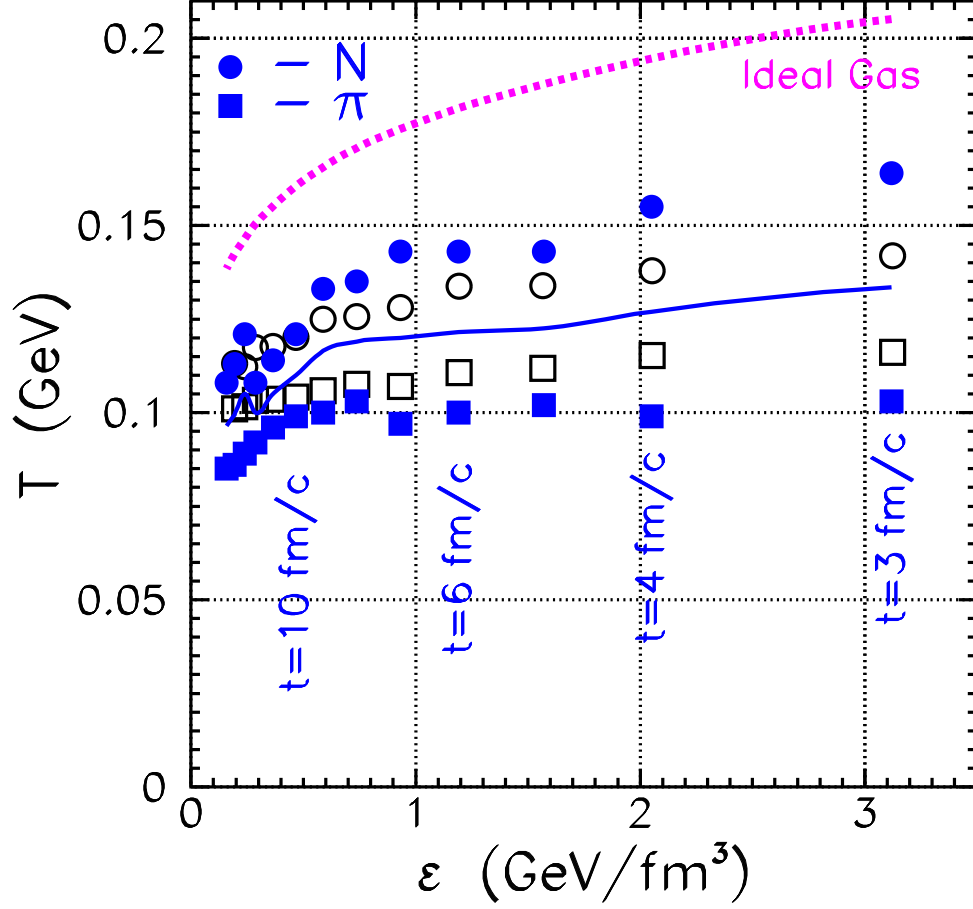


FIG. 10. Time evolution of energy density and temperature in the central cell of central Pb+Pb collisions at 160A GeV (full symbols) compared to the equilibrated infinite hadron matter (open symbols) and to the predictions of the ideal gas SM (dashed curve) calculated with the same ε , ρ_B , and ρ_S . Temperatures are extracted as the inverse slopes of Boltzmann fits to the energy spectra of nucleons (circles) and pions (squares). Solid curve indicates the average temperature of hadron mixture in the cell.

TABLES

TABLE I. The mean total energy, \sqrt{s} , of elastic and inelastic collisions in the box with $V = 125 \text{ fm}^3$, $\varepsilon = 468 \text{ MeV}/\text{fm}^3$, $\rho_B = 0.0924 \text{ fm}^{-3}$, and $\rho_S = -0.00987 \text{ fm}^{-3}$ at the quasiequilibrium stage. Of each pair of numbers for inelastic collisions the upper one corresponds to the reaction channel via the string excitations (S), and the lower one corresponds to the resonance excitation reactions (R).

| Type of reaction | | N_{react} (%) | \sqrt{s} (GeV) |
|------------------------------|---------------|------------------------|------------------|
| all reactions (100%) | inelas., S | 10 | 1.9 |
| | inelas., R | 35 | 1.1 |
| | elastic, tot. | 27 | 1.34 |
| | B decays | 8 | 1.36 |
| | M decays | 20 | 0.81 |
| baryon-baryon (BB) (100%) | inelas., S | 1 | 4.2 |
| | inelas., R | 32 | 2.7 |
| | elastic, tot. | 67 | 2.7 |
| meson-meson (MM) (100%) | inelas., S | 10 | 1.6 |
| | inelas., R | 54 | 0.8 |
| | elastic, tot. | 36 | 0.91 |
| meson-baryon (MB) (100%) | inelas., S | 25 | 2.1 |
| | inelas., R | 46 | 1.4 |
| | elastic, tot. | 29 | 2.0 |

TABLE II. The temperature T_{SM}^{all} extracted from the SM fit to UrQMD data at given ε , ρ_B , and ρ_S (determined from the cell), together with the temperature of nucleons $T_{\text{cell/box}}^N$ and pions $T_{\text{cell/box}}^\pi$ obtained by the Boltzmann fit to energy spectra of particles at 160A GeV within the time interval $10 \text{ fm}/c \leq t \leq 15 \text{ fm}/c$ in the central cell/box.

| time fm/c | T_{SM}^{all} MeV | T_{cell}^N MeV | T_{box}^N MeV | T_{cell}^π MeV | T_{box}^π MeV |
|--------------|------------------------------|----------------------------|---------------------------|------------------------------|-----------------------------|
| 10 | 160.6 | 121 | 125 | 99 | 106 |
| 11 | 155.2 | 114 | 120 | 96 | 104 |
| 12 | 150.5 | 108 | 118 | 92 | 104 |
| 13 | 146.5 | 121 | 117 | 89 | 103 |
| 14 | 142.4 | 113 | 112 | 86 | 102 |
| 15 | 138.5 | 108 | 113 | 85 | 101 |

TABLE III. The mean number of elastic collisions ($N_{\text{elas.}}$), inelastic reactions proceeding via the string fragmentations ($N_{\text{inel.}}^S$) and resonance decays ($N_{\text{inel.}}^R$), and via other inelastic channels ($N_{\text{inel.}}^{\text{other}}$) per fm/ c in the UrQMD box with $V = 125 \text{ fm}^3$ at the quasiequilibrium stage. Energy density, baryon density, and strangeness density in the box are the same as those in the central cell in central Au+Au (Pb+Pb) collisions at AGS (SPS) energy at $t = 13$ (10) fm/ c .

| Final mult. | AGS ($t = 13 \text{ fm}/c$) | | | | SPS ($t = 10 \text{ fm}/c$) | | | |
|----------------|----------------------------------|----------------------|----------------------|-----------------------------------|----------------------------------|----------------------|----------------------|-----------------------------------|
| | $N_{\text{elas.}}$ | $N_{\text{inel.}}^S$ | $N_{\text{inel.}}^R$ | $N_{\text{inel.}}^{\text{other}}$ | $N_{\text{elas.}}$ | $N_{\text{inel.}}^S$ | $N_{\text{inel.}}^R$ | $N_{\text{inel.}}^{\text{other}}$ |
| 1 | | | | 36.94 | | | | 170.26 |
| 2 | 30.14 | 2.26 | 33.05 | 11.91 | 151.83 | 17.87 | 130.61 | 3.773 |
| 3 | | 2.32 | 0.65 | | | 32.57 | 1.907 | |
| 4 | | 0.067 | 0.037 | | | 0.81 | 0.520 | |
| 5 | | 0.004 | | | | 0.04 | | |
| 6 | | 0.002 | | | | 0.01 | | |